Whistler influence on the overall VLF wave intensity in the upper ionosphere

J. Záhlava, F. Němec, Jean-Louis Pinçon, O. Santolík, I. Kolmašová, Michel Parrot

Whistler Influence on the Overall Very Low Frequency Wave Intensity in the Upper Ionosphere

Correspondence to:
J. Záhlava,
jan.zahlava@gmail.com

J. Záhlava[1] , **F. Němec[1]** , **J. L. Pincon[2]** , **O. Santolík[1,3]** , **I. Kolmašová[1,3]** , and **M. Parrot[2]**

[1]Faculty of Mathematics and Physics, Charles University, Prague, Czech Republic, [2]LPC2E/CNRS, Orléans, France, [3]Department of Space Physics, Institute of Atmospheric Physics, The Czech Academy of Sciences, Prague, Czech Republic

Abstract   We investigate the influence of lightning-generated whistlers on the overall intensity of electromagnetic waves measured by the Detection of Electro-Magnetic Emissions Transmitted from Earthquake Regions spacecraft (2004–2010, quasi Sun-synchronous polar orbit with an altitude of about 700 km) at frequencies below 18 kHz. Whistler occurrence rate evaluated using an onboard neural network designed for automated whistler detection is used to distinguish periods of high and low whistler occurrence rates. It is shown that especially during the night and particularly in the frequency-geomagnetic latitude intervals with a low average wave intensity, contribution of lightning-generated whistlers to the overall wave intensity is significant. At frequencies below 1 kHz, where all six electromagnetic wave components were measured during specific intervals, the study is accompanied by analysis of wave propagation directions. When we limit the analysis only to fractional-hop whistlers, which propagate away from the Earth, we find a reasonable agreement with results obtained from the whole data set. This also confirms the validity of the whistler occurrence rate analysis at higher frequencies.

1. Introduction

Very low frequency (VLF, up to about 30 kHz) electromagnetic waves observed in the upper ionosphere by low-altitude satellites may have different possible origins. They may be naturally generated in the magnetosphere by wave-particle interactions at larger radial distances, such as chorus (e.g., Masson et al., 2009; Omura et al., 1991; Santolík et al., 2014; Sazhin & Hayakawa, 1992) or equatorial noise (e.g., Hrbáčková et al., 2015; Němec et al., 2005; Ma et al., 2013; Santolík et al., 2004). These waves can then propagate downward to the Earth (Chum & Santolík, 2005; Santolík & Parrot, 1998, 1999, 2000; Santolík, Chum, et al., 2006; Santolík et al., 2016). Alternatively, they may be of an artificial origin, such as electromagnetic signals from VLF transmitters (Cohen & Inan, 2012; Starks et al., 2008) or power line harmonic radiation (e.g., Dudkin et al., 2015; Němec et al., 2006, 2015). Finally, they may also be generated by lightning discharges.

In the present study, we will focus on electromagnetic waves caused by lightning activity, and we will attempt to evaluate their relative importance in terms of the intensity as compared to waves of other origins. Each lightning stroke produces a short pulse of electromagnetic emissions over a wide frequency range called spheric (sometimes spelled as *sferic*). A part of these emissions can escape from the Earth-ionosphere waveguide and propagate through the plasma environment to higher altitudes (Fišer et al., 2010; Santolík & Parrot, 1996, 1998; Santolík et al., 2009; Walker, 1976). Considering that plasma is a dispersive medium, the group velocity of waves is a function of their frequency. In the case of the whistler mode, and for frequencies at small fractions of the electron cyclotron frequency, higher frequencies correspond to larger group velocities. Consequently, the lightning-produced waves transform into whistlers, that is, electromagnetic emissions whose lower frequencies arrive to the receiver later than their higher frequencies (Storey, 1953). The wave propagation is then either ducted or unducted (Green & Inan, 2006). The ducted waves propagate nearly parallel to the ambient magnetic field line in a duct consisting of a plasma with a slightly different density (Helliwell, 1965). Such waves can be then detected in the hemisphere opposite to the hemisphere in which they originated, in the magnetically conjugated point. On the other hand, the propagation of unducted waves is governed by gradients of the refractive index of the plasma medium (Budden, 1961).

Whistler formation and their usage for the derivation of plasma parameters were demonstrated by Storey (1953). A valuable overview of whistler experiments along with the relevant theory was given by Helliwell (1965, 2014). Besides the calculations of electron densities in the Earth's plasma environment (Carpenter, 1983;

Carpenter & Anderson, 1992), whistlers are also particularly important for their influence on the population of energetic particles in the Van Allen radiation belts. Specifically, they may result in a significant pitch angle scattering of energetic electrons, leading to their subsequent precipitation (Bortnik et al., 2006a, 2006b; Inan et al., 2007; Voss et al., 1998). Whistlers can also substantially contribute to the overall wave intensity in the magnetosphere. Especially during the night, when the wave attenuation in the ionosphere is lower (Cohen et al., 2012; Graf et al., 2013; Němec et al., 2008; Tao et al., 2010), it seems that the influence of lightning-generated whistlers is rather significant (Colman & Starks, 2013; Němec et al., 2010). However, the exact evaluation of the contribution of lightning-generated whistler waves to the total wave intensity is still an open question (Green et al., 2005; Green & Inan, 2006; Meredith et al., 2006; Thorne et al., 2006). An exciting recent development in studying whistlers is the automatic whistler detection and analysis network (e.g., Lichtenberger et al., 2010, 2013; Singh et al., 2014). Their approach allows for a nearly real-time plasmasphere sensing using the fully automated analysis of whistlers.

We use a neural network for whistler detection on board the low-altitude Detection of Electro-Magnetic Emissions Transmitted from Earthquake Regions (DEMETER) spacecraft along with simultaneous measurements of VLF wave intensity to evaluate the whistler influence on the overall wave intensity in the upper ionosphere. The data set is described in section 2. The obtained results are presented in section 3, and they are discussed in section 4. Finally, section 5 contains a brief summary.

2. Data Set

The French spacecraft DEMETER operated between July 2004 and December 2010. The measurements covered the regions between about −65° and 65° of the dipole geomagnetic latitude (evaluated at the spacecraft location; Lagoutte et al., 2005). The orbit of the spacecraft had an altitude of about 700 km, and it was nearly polar and quasi Sun-synchronous. Consequently, the measurements were performed in two distinct local time intervals, around 10:30 LT and around 22:30 LT. The exact distribution of the local times of DEMETER measurements is depicted in Figure 1 of Němec et al. (2010). Further, the local time interval about 10:30 LT is referred to as *day*, and the local time interval about 22:30 LT is referred to as *night*.

The instruments on board DEMETER performed both electric field (Berthelier et al., 2006) and magnetic field (Parrot et al., 2006) measurements. Depending on the frequency range and the spacecraft mode, a wide range of data sets is available. In the VLF range (up to 20 kHz), onboard calculated frequency-time spectrograms of power spectral density of one electric and one magnetic field component were always available. However, the magnetic field data in this frequency range contain a nonnegligible amount of spacecraft interferences, and therefore, in the VLF range, only electric field measurements are used in the present study. The measured frequency-time spectrograms have a time resolution of 2.048 s and a frequency resolution of 19.53 Hz. In the extralow-frequency (ELF) range (up to 1.25 kHz), high-resolution data are available during a sporadically active burst mode. They consist of waveforms of all six electromagnetic field components sampled at 2.5 kHz. A detailed wave analysis is therefore possible, and many wave parameters can be calculated as described, for example, by Santolík et al. (2003) and Santolík, Němec, et al. (2006). The availability of a predominant Poynting vector direction is particularly important for the present study.

Figure 1 shows color-coded geomagnetic maps with 1° × 1° resolution of the total duration of daytime (a) survey and (b) burst mode measurements. The magnetic dipole coordinate system is used. The nighttime coverage is approximately the same (not shown). The white color represents areas where no measurement was made. The histograms on the left show the total durations of measurements as a function of geomagnetic latitude, again with 1° resolution. It can be seen that the latitudinal coverage of the survey mode data is nearly homogeneous, while the burst mode data coverage peaks at midlatitude in the Northern Hemisphere. Overall, we use the data obtained during 25,960 daytime and 25,660 nighttime half orbits.

The DEMETER spacecraft was also equipped with an onboard neural network designed for the detection and classification of lightning-generated whistlers (Elie et al., 1999). High-resolution frequency-time spectrograms in the frequency range between 3 and 18 kHz were automatically searched for the presence of frequency-time patterns corresponding to whistlers. Based on manually analyzed spectrograms, which served as a learning data set for the neural network, whistlers were identified and classified into 19 dispersion classes. The time resolution of the resulting data (number of whistlers in each dispersion class) is 0.1024 s, and the time of an event corresponds to the time of arrival of a hypothetical nondispersed wave packet propagating at the speed
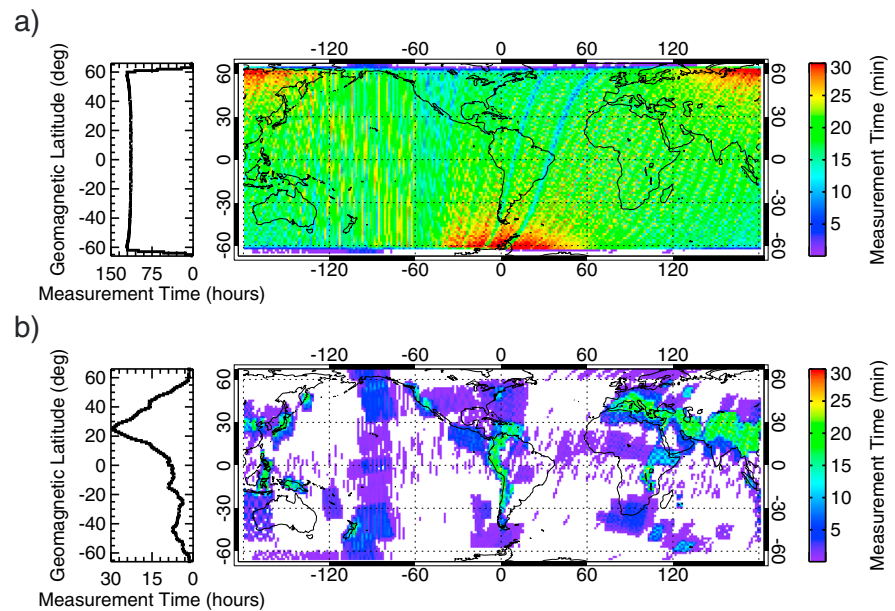
Figure 1. (a) Geomagnetic map of the total duration of daytime survey mode measurements. The magnetic dipole coordinate system is used. The measurement duration in individual 1°× 1° bins are color coded according to the scale on the right-hand side. The histogram on the left shows the total duration of daytime survey mode measurement as a function of geomagnetic latitude with 1° resolution. (b) The same as (a), but for the burst mode data.

of light. The first months of the DEMETER mission were used for the neural network learning process, and thus the neural network data are only available from May 2005.

Altogether, about 117 and 509 million whistlers were detected by the neural network during the daytime and nighttime half orbits, respectively. At the times when the burst mode was active, about 12.5 and 51.5 million whistlers were detected during the daytime and nighttime, respectively, that is, approximately 10% of the total number of detected whistlers. Detected whistlers with dispersion less than 10 $s^{1/2}$ (dispersion classes 0-6) correspond to fractional-hop whistlers (further called *0+ whistlers*; Smith & Angerami, 1968). An analysis of geographic distribution of whistlers in individual dispersion classes has been done. Specifically, whistlers with dispersions larger than 10 $s^{1/2}$ are detected in magnetically conjugated areas (not shown). The 0+ whistlers form the vast majority of detected whistlers (over 85 %).

3. Results

The basic idea of our analysis is to use the data provided by the neural network on board DEMETER to distinguish the intervals with a significant whistler occurrence and the intervals when lightning-generated whistlers are nearly absent. We considered only 0+ whistlers, that is, whistlers which are detected in the same hemisphere as the source lightning, without any passage through the geomagnetic equator.

Two examples of DEMETER spacecraft observations during the burst mode are presented in Figures 2 and 3. Figures 2a and 3a show the power spectral density of electric field fluctuations measured in the VLF range. Figures 2b and 3b show the number of whistlers detected by the neural network as a function of the dispersion class and time. The remaining panels show the results of a detailed wave analysis, which requires multicomponent wave measurements available only in the ELF range. Frequency-time spectrograms of power spectral density of electric and magnetic field fluctuations in the ELF range are shown in Figures 2c, 3c, 2d, and 3d, respectively. The detailed wave analysis was performed only for frequency-time intervals with power spectral density of magnetic field fluctuations larger than 3×10^{-8} nT^2/Hz and for electric field fluctuations larger than 3×10^{-7} mV$^2 \cdot$m$^{-2} \cdot$Hz^{-1}. Figures 2e and 3e show the frequency-time plots of the Poynting vector component parallel to the ambient magnetic field normalized by its standard deviation (Santolík et al., 2001). The positive and negative values correspond to the propagation along the ambient magnetic field and opposite to the ambient magnetic field, respectively. Frequency-time plots of the ellipticity of magnetic field fluctuations are shown in Figures 2f and 3f. The values range from −1 to 1. Positive values correspond to right-handed
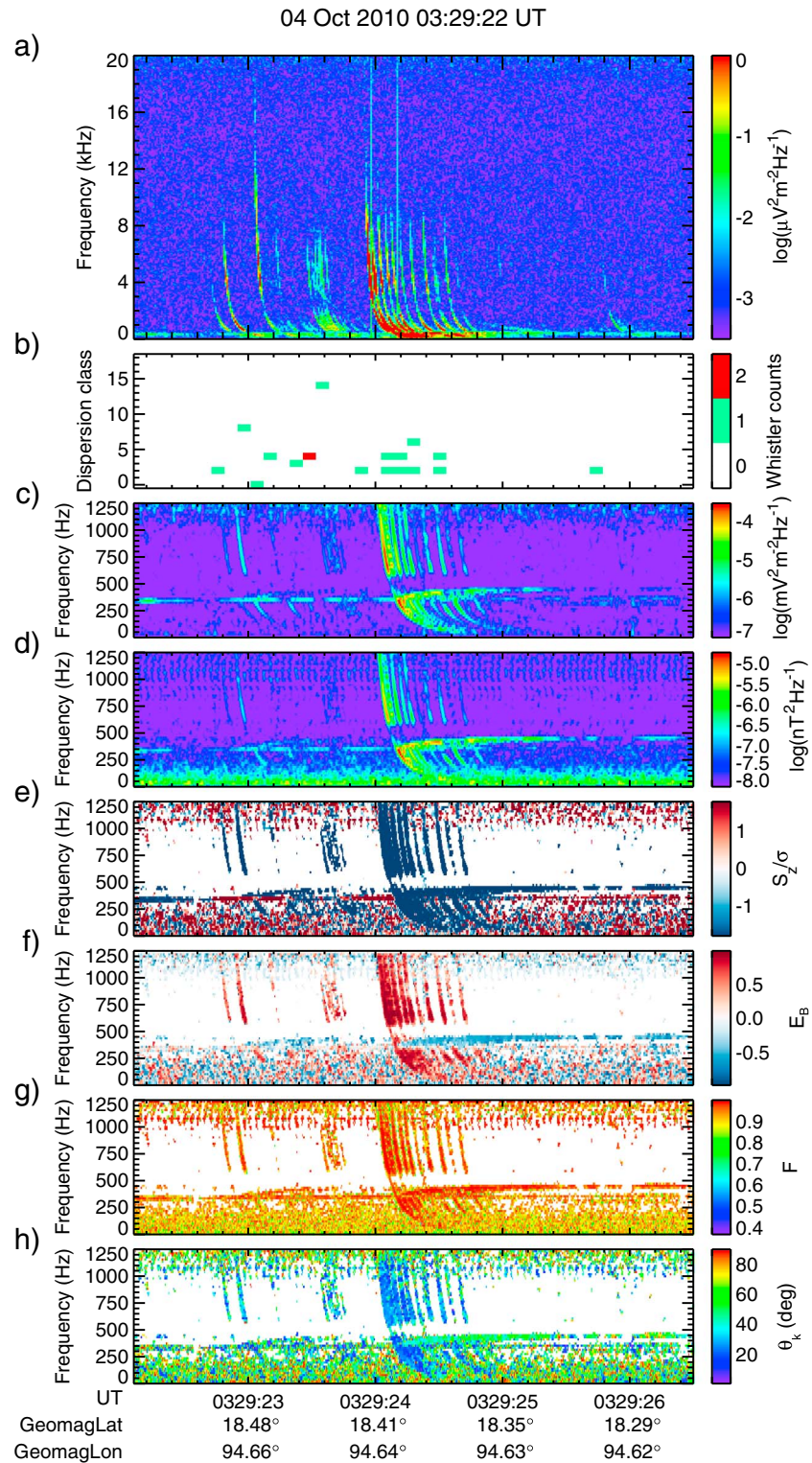
Figure 2. (a) Frequency-time spectrogram of power spectral density of electric field fluctuations measured in the VLF range. (b) Number of whistlers detected by the onboard neural network in each dispersion class. (c) Frequency-time spectrogram of electric field fluctuations measured in the ELF range. (d) Frequency-time spectrogram of magnetic field fluctuations measured in the ELF range. (e) Direction of the component of Poynting vector parallel to the ambient magnetic field normalized by its standard deviation. (f) Ellipticity of magnetic field fluctuations. (g) Planarity of magnetic field fluctuations. (h) Wave normal angle with respect to the ambient magnetic field. The measurements took place on 4 October 2010 between 03:29:22.1 UT and 03:29:26.5 UT during the local day. ELF = extralow-frequency.
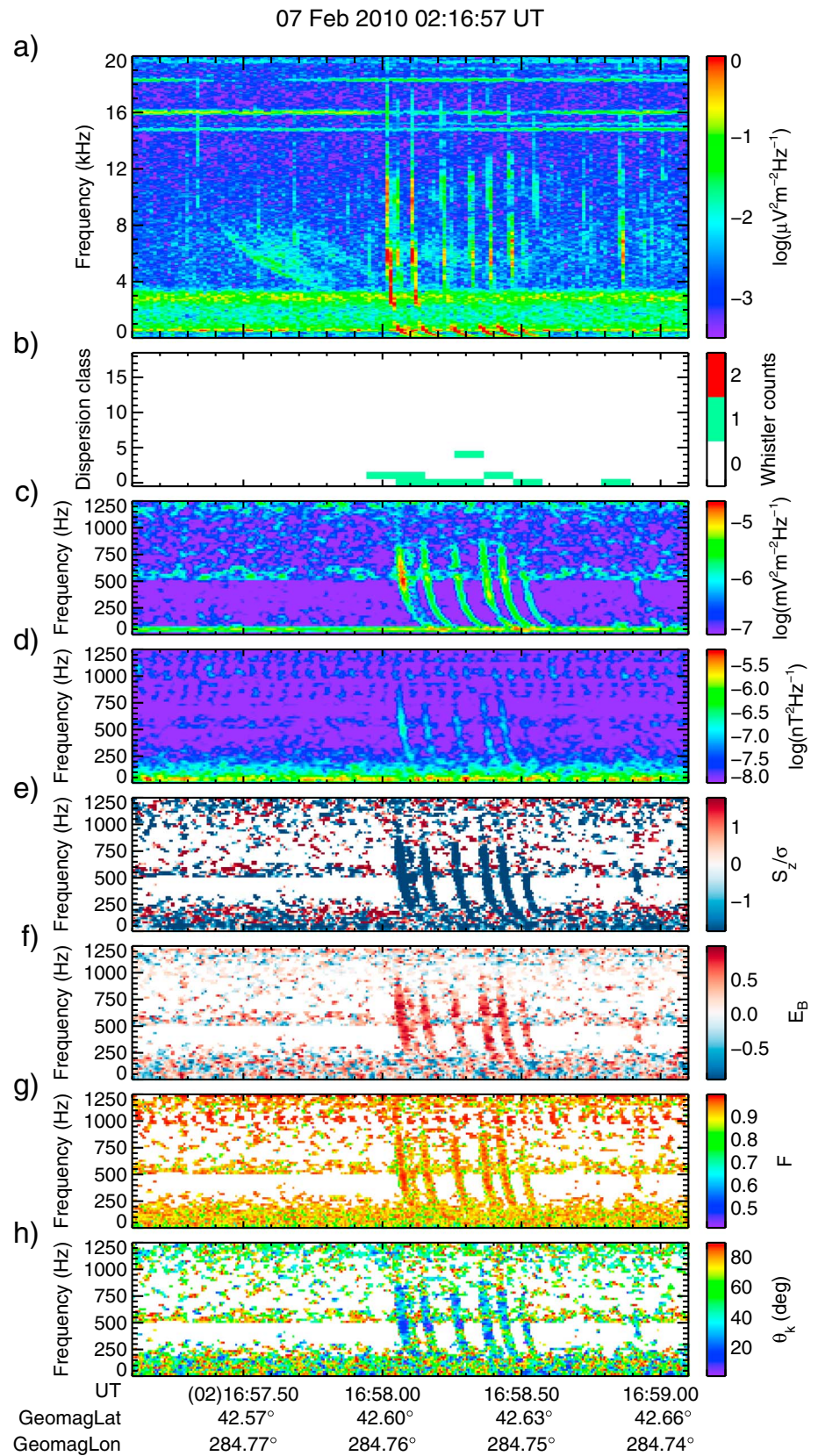
Figure 3. Same as Figure 2, but the measurements took place on 7 February 2010 from 02:16:57.4 UT to 02:16:59.4 UT corresponding to the local night.

polarized waves, while negative values correspond to left-handed polarized waves. The absolute value of ellipticity is calculated as a ratio of minor to major polarization axes, that is, circularly polarized waves have an ellipticity value of ±1, while linearly polarized waves have an ellipticity of 0 (Santolík & Gurnett, 2002). Figures 2g and 3g show the planarity of magnetic field fluctuations (Santolík et al., 2003), that is, how well the magnetic field fluctuations are confined to a single plane (planarity equal to 1). Finally, Figures 2h and 3h show the wave normal angle with respect to the ambient magnetic field calculated using the singular value decomposition method (Santolík et al., 2003). The data shown in Figure 2 were measured on 4 October 2010 from 03:29:22.1 UT to 03:29:26.5 UT during a daytime half orbit. At that time, DEMETER flew over the central Africa. Figure 3 depicts the measurements performed on 7 February 2010 from 02:16:57.4 UT to 02:16:59.4 UT during a nighttime half orbit. During this time interval, the spacecraft was located south of Alaska. During both measurement intervals, the spacecraft flew over the Northern Hemisphere.

Figures 2a and 2b show a comparison between the whistler activity and the numbers of detected whistlers. For most whistlers observed in Figure 2a, one can identify a point in Figure 2b, and vice versa, demonstrating a reasonable performance of the neural network. The whistlers that extend down to low frequencies are also visible in Figures 2c and 2d. This allows for the analysis of their propagation parameters (shown in panels e–h). They propagate in the direction opposite to the ambient magnetic field line, which in the Northern Hemisphere corresponds to the upward propagation from the Earth, as expected. All observed intense whistlers exhibit nearly right-hand circular polarization and low wave normal angles. Their planarity is close to 1, indicating a validity of the plane wave approximation. The background noise in Figure 3a is more significant than in Figure 2a. Some whistlers are therefore either hard to identify or split into several parts. At the beginning of the time interval, there is a high dispersion (multihop) whistler which occurs in the same frequency-time interval as two 0+ whistlers. This high-dispersion whistler probably made the 0+ whistlers undetectable for the neural network. Several whistlers extend down into the ELF range. They are found to propagate away from the Earth. The values of planarity are again close to 1. The waves propagate at low wave normal angles. The ellipticity at frequencies larger than about 250 Hz is close to 1 (circular, right-handed polarized wave), in agreement with the value expected for the whistler mode propagation.

The occurrence rates of 0+ whistlers as a function of the geomagnetic latitude are shown in Figure 4. Average whistler occurrence rates observed by the DEMETER spacecraft in individual 2.048 s time intervals (corresponding to the time resolution of VLF survey mode data) were used to construct the overall distributions of whistler occurrence rates gathered over the whole DEMETER mission. Separate distributions have been collected in 1° intervals of the absolute values of geomagnetic latitude and for the dayside and nightside half orbits. Then, 0.25, and 0.75 quantiles of those distributions were adopted as low/high whistler occurrence thresholds, respectively. Dark colored dots in Figure 4 correspond to the upper thresholds, and light colored triangles represent the lower thresholds. The thresholds for the nighttime half orbits are shown in blue, while the thresholds for the daytime half orbits are shown in red. Additionally, the median values are shown by the solid lines of the respective colors. It can be seen that the threshold values are larger during the night than during the day, that is, there are generally more whistlers detected during the nighttime. This is probably caused by two main factors: (i) for the timing of the DEMETER day and night observations, global lightning occurrence is on average ∼ 60% larger during the nighttime half orbits (Figure 3 of Colman & Starks, 2013), and (ii) attenuation in the ionosphere is significantly larger during the daytime than during the nighttime (Němec et al., 2008), and only powerful lightning strokes thus produce whistlers sufficiently intense to be detected. Detected whistler occurrence rates are generally larger than the numbers of lightning strokes per square degree (e.g., Rodger et al., 2009). This is probably caused by a contribution of lightning strokes occurring at distances as large as 1,000 km (Fišer et al., 2010). Moreover, the unducted whistlers might further enlarge this area in the latitudinal direction (e.g., Bortnik et al., 2003). The lightning occurrence rates are the largest at low latitudes (e.g., Figure 8a of Christian et al., 2003), which does not agree with the decreasing whistler occurrence rates toward the geomagnetic equator, shown in Figure 4. This discrepancy is probably caused by the latitudinal dependence of ionospheric attenuation. Specifically, due to the latitudinal dependence of magnetic field inclination, the attenuation is most significant around the geomagnetic equator, and it gradually decreases toward larger geomagnetic latitudes (e.g., Figures 3-35 of Helliwell, 1965). For the purpose of the VLF data classification, any whistler occurrence rate averaged over a 2.048 s interval larger than or equal to the upper threshold was considered as *high*. Similarly, any whistler occurrence rate averaged over a 2.048 s interval lower than or equal to the lower threshold was considered as *low*.
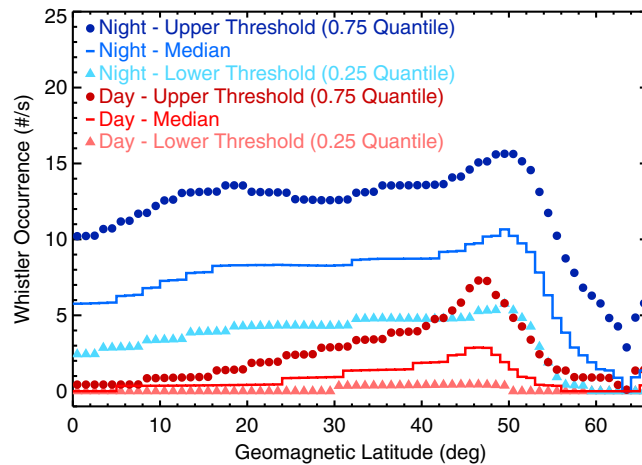
Figure 4. Quartiles of whistler occurrence rate as a function of the absolute value of the geomagnetic latitude. The daytime and nighttime values are represented by the red and blue colors, respectively. The 0.75 and 0.25 quantiles are shown by the dots and triangles, respectively. These are then, respectively, used as *high* and *low* whistler occurrence thresholds in the further analysis. Additionally, the solid lines of the respective colors represent the median values.

Figures 5a and 5b show median power spectral density of electric field fluctuations measured during the daytime half orbits as a function of frequency and the absolute value of geomagnetic latitude. Figure 5a was calculated using the data obtained at the times of high whistler occurrence rate, and Figure 5b was calculated using the data obtained at the times of low whistler occurrence rate. The color scale is the same for both figures in order to allow for an easy visual comparison. Both figures reveal high wave intensities at large geomagnetic latitudes and low frequencies up to about 1 kHz at the times of high whistler occurrence rate (Figure 5a) and up to about 2 kHz at the times of low whistler occurrence rate (Figure 5b). Figures 5c and 5d show median power
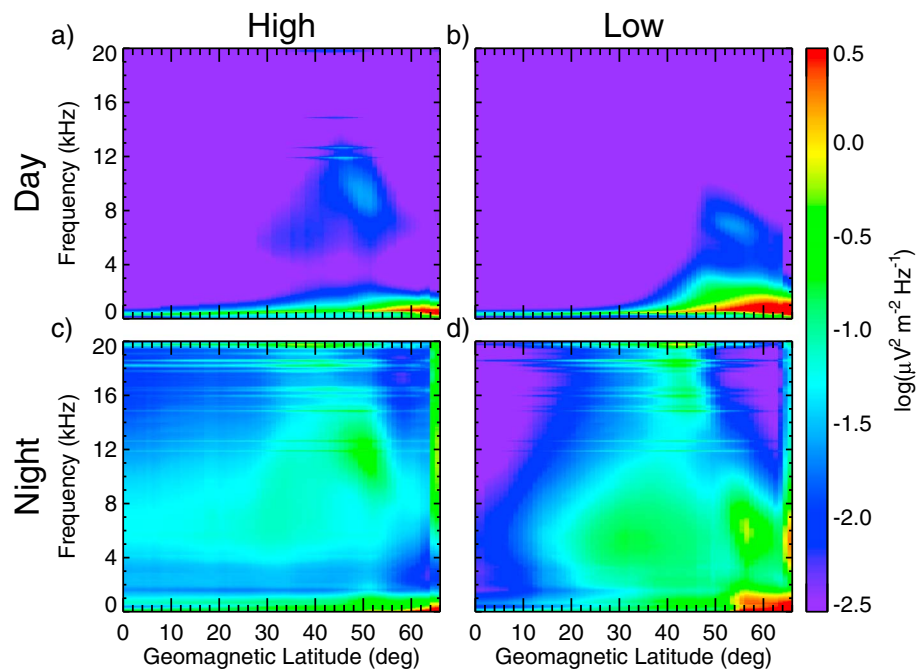
Figure 5. Color-coded median power spectral density of electric field fluctuations as a function of frequency and the absolute value of geomagnetic latitude. Results were obtained (a) at the times of high whistler occurrence rate during the daytime half orbits, (b) at the times of low whistler occurrence rate during the daytime half orbits, (c) at the times of high whistler occurrence rate during the nighttime half orbits, and (d) at the times of low whistler occurrence rate during the nighttime half orbits. The horizontal intense lines at frequencies above about 12 kHz observable especially during the night are due to very low frequency transmitters.
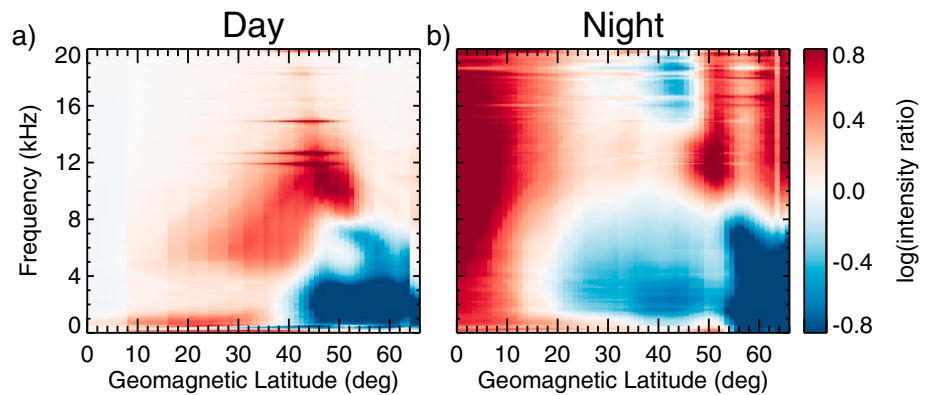
Figure 6. Color-coded ratio between the median power spectral density of electric field fluctuations during the high and low whistler occurrence rate periods. (a) Results obtained using the daytime half orbits. (b) Results obtained using the nighttime half orbits. The red color corresponds to the situation of larger median wave intensity at the times of high whistler occurrence. The blue color corresponds to the frequency-geomagnetic latitude intervals where the median wave intensity is larger at the times of low whistler occurrence. The red horizontal lines at frequencies about 12, 15, and 18 kHz observed in particular during the daytime correspond to very low frequency transmitter signals.

spectral density of electric field fluctuations at the times of high/low whistler occurrence rates, respectively, measured during the nighttime half orbits. The used format is the same as in Figures 5a and 5b. Similarly as during the day, there is a high intensity region at large latitudes and low frequencies during the night. In comparison to the daytime measurements, the region appears to be somewhat shifted to larger latitudes.

In order to evaluate the difference between the high and low whistler occurrence cases quantitatively, we have calculated a ratio of the respective median power spectral densities. The results are plotted in Figure 6, using a logarithmic color scale. Figure 6a was obtained for daytime half orbits, while Figure 6b was obtained for nighttime half orbits. Due to the used logarithmic scales, the power spectral density ratios plotted in Figures 6a and 6b effectively correspond to the differences between Figures 5a and 5b and between 5c and 5d, respectively. Large values of the intensity ratios correspond to the situation of a larger intensity observed at the times of higher whistler occurrence, indicating that the whistler contribution to the overall wave intensity was rather significant or that other types of intense waves are occurring at the same time as whistlers. On the other hand, low values of the intensity ratios correspond to the situation of a lower intensity observed at the times of higher whistler occurrence. This likely does not correspond to a situation of other waves being less intense due to the whistler occurrence, but it is probably linked to the properties of the whistler detection algorithm. Specifically, the number of detected whistlers is larger at the times of less intense wave background. Then, should the intensity of other waves be independent of the whistler occurrence, we might expect the intensity to be on average lower at the times of high whistler occurrence (when the identification algorithm works better). We shall discuss this more in detail in section 4. It can be seen that large areas of the plots in Figure 6 are covered in red, possibly owing to a significant contribution of whistlers to the overall wave intensity. Negative values of the intensity ratios (blue) are obtained especially at larger geomagnetic latitudes and lower frequencies (up to approximately 8 kHz). During the night, there is an additional area where the wave intensity ratio is negative, at frequencies between about 15 and 20 kHz, and at geomagnetic latitudes of about 30°–50°.

We will now focus on the ELF range, where all three electric and all three magnetic field components were measured with a sampling rate of 2.5 kHz in the burst mode and where full waveform data are available. It is thus possible to obtain detailed spectrograms showing individual whistlers and to perform a detailed wave analysis, and, most importantly, to calculate a predominant Poynting vector direction (Santolík & Parrot, 1998, 1999). The idea is to compare the results obtained using the whistler detection algorithm and the results obtained using distinction of waves by their propagation properties. Figures 7a and 7b show the ELF frequency range of Figures 6a and 6b, respectively, that is, the appropriate frequency intervals for which the wave analysis is possible. The intensity ratios in this frequency range exhibit a strong dependence on the geomagnetic latitude. At low latitudes, wave intensities associated with high whistler occurrence are larger than wave intensities associated with low whistler occurrence, but the difference gradually decreases toward larger geomagnetic latitudes. Finally, at latitudes larger than about 40° (or larger than 50° at frequencies below 250 Hz),
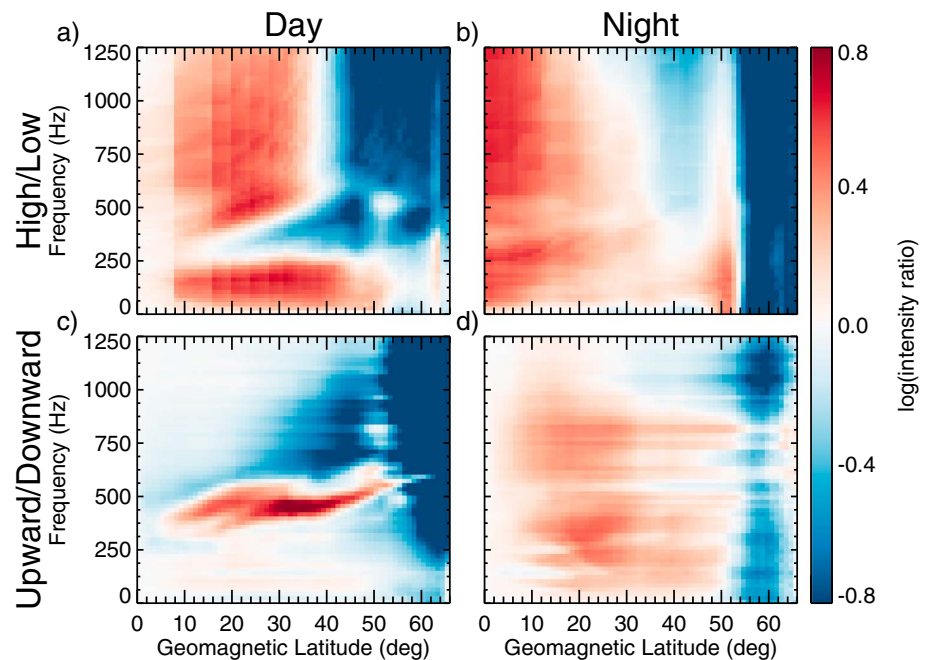
Figure 7. (a) Extremely low frequency part of Figure 6a (daytime). (b) Extremely low frequency part of Figure 6b (nighttime). (c, d) Color-coded ratio between the median power spectral density of electric field fluctuations of the waves propagating predominantly away from the Earth and those propagating predominantly toward the Earth. The results were obtained using the daytime (c) and nighttime (d) half orbits. The red color corresponds to the frequency-geomagnetic latitude intervals where the median wave intensity is larger for the upward propagation.

the intensity is larger during the low whistler occurrence period. During the daytime, one can also identify a region at frequencies between about 300 and 500 Hz and latitudes from 15° to 50° with wave intensities larger during the low whistler occurrence rate than during the high whistler occurrence rate. Figures 7c and 7d show the ratios between the median electric field intensities of the waves propagating upward and those propagating downward calculated for the daytime and nighttime, respectively. By the *upward* and *downward* propagation we mean that the component of the Poynting vector parallel to the ambient magnetic field is respectively directed away/toward the Earth. In Figures 7c and 7d, the red part of the color scale represents the intervals in which larger median intensities are associated with upward propagating waves. The blue color in Figures 7c and 7d corresponds to the situation of downward propagating waves being more intense than those propagating upward. Similarly as for the whistler occurrence rate analysis, the intensity ratios in Figures 7c and 7d also depend primarily on the geomagnetic latitude. Moreover, there is an area between about 300 and 500 Hz during the day, where the intensity of upgoing waves is significantly larger than the intensity of downgoing waves.

4. Discussion

In the first part of the present study, we used the data provided by the onboard neural network for whistler detection to classify the VLF electric field power spectral densities according to whether they were observed at the times of low/high whistler occurrence rate. The thresholds for the whistler occurrence rate to be considered as low/high were determined separately for day and night, and for each 1° interval of the absolute value of geomagnetic latitude. This distinction allows us to properly select the times with unusually low/high whistler occurrence rate as compared to the normal situation in a given latitude-local time interval. Only 0+ whistlers are considered in the analysis, which significantly facilitates the interpretation of the obtained results. These were distinguished based on the dispersion class identified by the neural network. Note that this restriction of the analysis to 0+ whistlers removes less than 15% of the total number of detected whistlers (see section 2).

Power spectral density of electric field fluctuations at frequencies above 1 kHz is typically larger during the nighttime than during the daytime. This may indicate a significant influence of lightning-generated whistlers

in most of the analyzed frequency-latitude intervals, considering they are more attenuated in the ionosphere during the day than during the night.

A comparison of the results obtained during high and low whistler occurrence rate reveals that there are frequency-latitude intervals where the wave intensity is larger during the high whistler occurrence rate than during the low whistler occurrence rate, as well as intervals exhibiting the opposite behavior. Unfortunately, interpretation of the difference between the high and low whistler occurrence results is not straightforward. The reason is the varying efficiency of the whistler detection algorithm. If it was not caused by the efficiency dependence, the wave intensity detected during the high whistler occurrence rate would be larger than the intensity detected during the low whistler occurrence rate in all intervals, as the lightning-generated whistlers can only add their contribution to the overall detected wave intensity. However, it appears that the whistler detection algorithm works noticeably better at the times of lower background wave intensity. Unfortunately, we do not believe a quantitative evaluation of the neural network whistler detection efficiency has been undertaken at the present time. Considering the lower whistler detection efficiency at the times of high intensity background, waves generated by other sources than lightning should be on average more intense during the low whistler occurrence rate periods. In order to obtain larger wave intensity at the times of high whistler occurrence rate, the lightning-generated whistler contribution thus has to be rather significant to overcome this detection bias or other types of waves need to occur at the same time as whistlers. Focusing on Figure 6, it can be seen that the red areas (representing larger wave intensity at the times of higher whistler occurrence rate) are preferably distributed in the areas where the long-term average wave intensity is generally lower in Figures 5a–5d. On the other hand, the blue areas (representing larger wave intensity at the times of lower whistler occurrence rate) are typically found in frequency-latitude intervals with the largest long-term average power spectral density of electric field fluctuations.

A plausible hypothesis therefore is that the whistler contribution to the overall wave intensity is significant in the red frequency-latitude intervals in Figure 6. On the other hand, in the blue frequency-latitude intervals waves of nonlightning origin dominate. Whistlers appear to be most important for the overall wave intensity during the night at low to midgeomagnetic latitudes at frequencies above about 8 kHz. On the other hand, non–lightning-generated natural emissions have the largest influence at low frequencies and at larger geomagnetic latitudes. This is roughly consistent with Figures 6 and 7 of Němec et al. (2010) obtained by comparing summer and winter periods at geomagnetic longitudes of North America. It is also worth mentioning that the spectral lines corresponding to the signals coming from powerful terrestrial VLF transmitters are shown in dark red in Figure 6. Although the overall intensity of transmitter signals is generally lower during the daytime than during the nighttime due to the larger attenuation in the ionosphere (shown also, e.g., by Gamble et al., 2008), its variation with whistler occurrence rate is especially evident during the daytime (Figure 6a). Specifically, their intensity is larger at the times of the high whistler occurrence rate than that at the times of the low whistler occurrence rate. We suggest two possible hypotheses: (i) The VLF transmitters might influence the ionosphere making it more penetrable for signals generated by lightning. More whistlers would be thus detected in the areas influenced by the transmitters, and subsequently, the high whistler occurrence rates would be associated with the enhanced wave intensity at the transmitter frequencies. (ii) The ionospheric attenuation plays an important role in the coupling between VLF waves on the ground (both lightning and transmitter generated), and the signals are thus likely observed by the satellite. More whistlers and stronger transmitter signals would be then detected at the times when the ionospheric attenuation is lower. As the ionospheric attenuation is generally much lower during the night than during the day, these explanations would be consistent with the effect occurring predominantly during the day.

In the ELF range, results obtained by the whistler occurrence rate analysis were compared to the results obtained by the analysis based on the Poynting vector directions. The analysis based on the Poynting vector directions, however, has its own drawbacks. First, only the predominant Poynting vector direction is obtained and waves of both directions might be present in a given bin of Figures 7b and 7d. Second, not all upward propagating waves are of the terrestrial origin, because it is also possible that the waves generated at larger distances are reflected at lower altitudes, and then thus apparently propagate upward. The reflected waves may be, however, expected to be less intense than the downward propagating waves. Consequently, when detecting simultaneously both downgoing and upgoing (refracted) waves without any contribution of the terrestrial sources, the resulting Poynting vector should be on average oriented toward the Earth. For the comparison of the results obtained using the two approaches, the fact that only 0+ whistlers identified by the neural network were included in the analysis in the previous part becomes very important. As 0+ whistlers

originate in the same hemisphere in which they are observed, their Poynting vector is oriented upward, that is, away from the Earth. It is therefore possible to directly compare the two results. One could argue that the results obtained using the VLF survey mode data and the whistler occurrence rate analysis might be different when restricted only to the burst mode locations due to a selection bias. We thus performed the same analysis limited only to the time intervals with an active burst mode. The results obtained for this reduced data set are principally the same as the results obtained using the full survey mode time intervals (not shown). Despite all the imperfections, the comparison depicted in Figures 7a and 7b and Figures 7c and 7d shows a rather good agreement between the two methods. There is, however, a significant discrepancy during the daytime in the frequency range between 300 and 500 Hz. The whistler occurrence rate analysis shows that whistlers do not contribute in this frequency-latitude interval, whereas the Poynting vector direction method shows a larger wave intensity associated with the upward propagation. Note that the frequency range of this discrepancy area is not constant, but it moves to higher frequencies at larger geomagnetic latitudes. Although propagating upward, these waves most probably do not come from lightning nor any other terrestrial source. The observed phenomenon is likely the one described by Santolík and Parrot (1999) as *type F waves* which originate in hiss/chorus propagating downward at larger latitudes, reflecting subsequently at the two-ion cutoff frequency toward lower latitudes (Santolík, Chum, et al., 2006).

5. Summary

We used two different approaches to investigate the contribution of lightning-generated whistlers to the overall wave intensity of electromagnetic waves measured in terms of the power spectral density of electric field fluctuations by the DEMETER spacecraft at an altitude of about 700 km. Using the onboard neural network designed for whistler detection, we have identified intervals of frequency and geomagnetic latitude where the whistlers predominantly occur and where the wave intensities are high at the same time. This analysis has been done both during the day and during the night. In the ELF range, the results of the whistler occurrence rate analysis were compared to the results obtained by the analysis of the Poynting vector directions, showing a reasonable agreement. The observed discrepancies can be explained in terms of the waves generated at larger radial distances reflected at the multi-ion cutoff frequency at larger geomagnetic latitudes, and thus propagating apparently away from the Earth.

References

Berthelier, J.-J., Godefroy, M., Leblanc, F., Malingre, M., Menvielle, M., Lagoutte, D., et al. (2006). ICE, the electric field experiment on DEMETER. *Planetary and Space Science*, *54*(5), 456–471. https://doi.org/10.1016/j.pss.2005.10.016

Bortnik, J., Inan, U. S., & Bell, T. F. (2003). Energy distribution and lifetime of magnetospherically reflecting whistlers in the plasmasphere. *Journal of Geophysical Research*, *108*(A5), 1199. https://doi.org/10.1029/2002JA009316

Bortnik, J., Inan, U. S., & Bell, T. F. (2006a). Temporal signatures of radiation belt electron precipitation induced by lightning-generated MR whistler waves: 1. Methodology. *Journal of Geophysical Research*, *111*, A02204. https://doi.org/10.1029/2005JA011182

Bortnik, J., Inan, U. S., & Bell, T. F. (2006b). Temporal signatures of radiation belt electron precipitation induced by lightning-generated MR whistler waves: 2. Global signatures. *Journal of Geophysical Research*, *111*, 2205. https://doi.org/10.1029/2005JA011398

Budden, K. G. (1961). *The wave-guide mode theory of wave propagation*. Michigan: Logos Press.

Carpenter, D. L. (1983). Some aspects of plasmapause probing by whistlers. *Radio Science*, *18*(6), 917–925. https://doi.org/10.1029/RS018i006p00917

Carpenter, D., & Anderson, R. (1992). An ISEE/whistler model of equatorial electron density in the magnetosphere. *Journal of Geophysical Research*, *97*(A2), 1097–1108. https://doi.org/10.1029/91JA01548

Christian, H. J., Blakeslee, R. J., Boccippio, D. J., Boeck, W. L., Buechler, D. E., Driscoll, K. T., et al. (2003). Global frequency and distribution of lightning as observed from space by the Optical Transient Detector. *Journal of Geophysical Research*, *108*(D1), 4005. https://doi.org/10.1029/2002JD002347

Chum, J., & Santolík, O. (2005). Propagation of whistler-mode chorus to low altitudes: Divergent ray trajectories and ground accessibility. *Annales Geophysicae*, *23*(12), 3727–3738. https://doi.org/10.5194/angeo-23-3727-2005

Cohen, M. B., & Inan, U. (2012). Terrestrial VLF transmitter injection into the magnetosphere. *Journal of Geophysical Research*, *117*, A08310. https://doi.org/10.1029/2012JA017992

Cohen, M. B., Lehtinen, N. G., & Inan, U. S. (2012). Models of ionospheric VLF absorption of powerful ground based transmitters. *Geophysical Research Letters*, *39*, L24101. https://doi.org/10.1029/2012GL054437

Colman, J., & Starks, M. (2013). VLF wave intensity in the plasmasphere due to tropospheric lightning. *Journal of Geophysical Research: Space Physics*, *118*, 4471–4482. https://doi.org/10.1002/jgra.50217

Dudkin, F., Korepanov, V., Dudkin, D., Pilipenko, V., Pronenko, V., & Klimov, S. (2015). Electric field of the power terrestrial sources observed by microsatellite Chibis-M in the Earth's ionosphere in frequency range 1–60 Hz. *Geophysical Research Letters*, *42*, 5686–5693. https://doi.org/10.1002/2015GL064595

Elie, F., Hayakawa, M., Parrot, M., Pinçon, J.-L., & Lefeuvre, F. (1999). Neural network system for the analysis of transient phenomena on board the DEMETER micro-satellite. *IEICE TRANSACTIONS on Fundamentals of Electronics, Communications and Computer Sciences*, *82*(8), 1575–1581.

Fišer, J., Chum, J., Diendorfer, G., Parrot, M., & Santolík, O. (2010). Whistler intensities above thunderstorms. *Annales Geophysicae*, *28*, 37–46. Copernicus GmbH https://doi.org/10.5194/angeo-28-37-2010

Gamble, R. J., Rodger, C. J., Clilverd, M. A., Sauvaud, J.-A., Thomson, N. R., Stewart, S., et al. (2008). Radiation belt electron precipitation by man-made VLF transmissions. *Journal of Geophysical Research*, *113*, A10211. https://doi.org/10.1029/2008JA013369

Graf, K., Lehtinen, N., Spasojevic, M., Cohen, M., Marshall, R., & Inan, U. (2013). Analysis of experimentally validated trans-ionospheric attenuation estimates of VLF signals. *Journal of Geophysical Research: Space Physics*, *118*, 2708–2720. https://doi.org/10.1002/jgra.50228

Green, J. L., Boardsen, S., Garcia, L., Taylor, W., Fung, S. F., & Reinisch, B. (2005). On the origin of whistler mode radiation in the plasmasphere. *Journal of Geophysical Research*, *110*, A03201. https://doi.org/10.1029/2004JA010495

Green, J. L., & Inan, U. (2006). Chapter 4: Lightning effects on space plasmas and applications. In C. Grabbe (Ed.), *Plasma physics applied* (pp. 59–72). Scarborough, Ontario, Canada: Transworld Research Network.

Helliwell, R. A. (1965). *Whistlers and related ionospheric phenomena* (Vol. 50). Stanford, CA: Stanford University Press Stanford.

Helliwell, R. A. (2014). *Whistlers and related ionospheric phenomena (Dover Books on Electrical Engineering)*. Mineola: Dover Publications.

Hrbáčková, Z., Santolík, O., Němec, F., Macúšová, E., & Cornilleau-Wehrlin, N. (2015). Systematic analysis of occurrence of equatorial noise emissions using 10 years of data from the Cluster mission. *Journal of Geophysical Research: Space Physics*, *120*, 1007–1021. https://doi.org/10.1002/2014JA020268

Inan, U. S., Piddyachiy, D., Peter, W. B., Sauvaud, J. A., & Parrot, M. (2007). DEMETER satellite observations of lightning-induced electron precipitation. *Geophysical Research Letters*, *34*, L07103. https://doi.org/10.1029/2006GL029238

Lagoutte, D., Brochot, J. Y., de Carvalho, D., Madrias, L., & Parrot, M. (2005). DEMETER microsatellite–Scientific Mission Center–Data product description, Lab. Phys. et Chimie de l'Environ., Orléans, France. DMT-SP-9-CM-6054-LPC, Technical Note.

Lichtenberger, J., Clilverd, M. A., Heilig, B., Vellante, M., Manninen, J., Rodger, C. J., et al. (2013). The plasmasphere during a space weather event: First results from the PLASMON project. *Journal of Space Weather and Space Climate*, *3*, A23. https://doi.org/10.1051/swsc/2013045

Lichtenberger, J., Ferencz, C., Hamar, D., Steinbach, P., Rodger, C. J., Clilverd, M. A., & Collier, A. B. (2010). Automatic whistler detector and analyzer system: Implementation of the analyzer algorithm. *Journal of Geophysical Research*, *115*, A12214. https://doi.org/10.1029/2010JA015931

Ma, Q., Li, W., Thorne, R. M., & Angelopoulos, V. (2013). Global distribution of equatorial magnetosonic waves observed by THEMIS. *Geophysical Research Letters*, *40*, 1895–1901. https://doi.org/10.1002/grl.50434

Masson, A., Santolík, O., Carpenter, D. L., Darrouzet, F., Décréau, P. M., Mazouz, F. E.-L., et al. (2009). Advances in plasmaspheric wave research with CLUSTER and IMAGE observations. In *The Earth's plasmasphere* (pp. 137–191). New York: Springer. https://doi.org/10.1007/s11214-009-9508-7

Meredith, N. P., Horne, R. B., Clilverd, M. A., Horsfall, D., Thorne, R. M., & Anderson, R. R. (2006). Origins of plasmaspheric hiss. *Journal of Geophysical Research*, *111*, A09217. https://doi.org/10.1029/2006JA011707

Němec, F., Parrot, M., & Santolík, O. (2015). Power line harmonic radiation observed by the DEMETER spacecraft at 50/60 Hz and low harmonics. *Journal of Geophysical Research: Space Physics*, *120*, 8954–8967. https://doi.org/10.1002/2015JA021682

Němec, F., Santolík, O., Gereová, K., Macúšová, E., De Conchy, Y., & Cornilleau-Wehrlin, N. (2005). Initial results of a survey of equatorial noise emissions observed by the Cluster spacecraft. *Planetary and Space Science*, *53*(1), 291–298. https://doi.org/10.1016/j.pss.2004.09.055

Němec, F., Santolík, O., Parrot, M., & Berthelier, J. (2006). Power line harmonic radiation (PLHR) observed by the DEMETER spacecraft. *Journal of Geophysical Research*, *111*, A04308. https://doi.org/10.1029/2005JA011480

Němec, F., Santolík, O., Parrot, M., & Bortnik, J. (2008). Power line harmonic radiation observed by satellite: Properties and propagation through the ionosphere. *Journal of Geophysical Research*, *113*, A08317. https://doi.org/10.1029/2008JA013184

Němec, F., Santolík, O., Parrot, M., & Rodger, C. (2010). Relationship between median intensities of electromagnetic emissions in the VLF range and lightning activity. *Journal of Geophysical Research*, *115*, A08315. https://doi.org/10.1029/2010JA015296

Omura, Y., Nunn, D., Matsumoto, H., & Rycroft, M. (1991). A review of observational, theoretical and numerical studies of VLF triggered emissions. *Journal of Atmospheric and Terrestrial Physics*, *53*(5), 351–368. https://doi.org/10.1016/0021-9169(91)90031-2

Parrot, M., Benoist, D., Berthelier, J., Blecki, J., Chapuis, Y., Colin, F., et al. (2006). The magnetic field experiment IMSC and its data processing onboard DEMETER: Scientific objectives, description and first results. *Planetary and Space Science*, *54*(5), 441–455. https://doi.org/10.1016/j.pss.2005.10.015

Rodger, C. J., Lichtenberger, J., McDowell, G., & Thomson, N. R. (2009). Automatic whistler detection: Operational results from New Zealand. *Radio Science*, *44*, RS2004. https://doi.org/10.1029/2008RS003957

Santolík, O., Chum, J., Parrot, M., Gurnett, D., Pickett, J., & Cornilleau-Wehrlin, N. (2006). Propagation of whistler mode chorus to low altitudes: Spacecraft observations of structured ELF hiss. *Journal of Geophysical Research*, *111*, A10208. https://doi.org/10.1029/2005JA011462

Santolík, O., & Gurnett, D. (2002). Propagation of auroral hiss at high altitudes. *Geophysical research letters*, *29*(10), 1481. https://doi.org/10.1029/2001GL013666

Santolík, O., Lefeuvre, F., Parrot, M., & Rauch, J. (2001). Complete wave-vector directions of electromagnetic emissions: Application to INTERBALL-2 measurements in the nightside auroral zone. *Journal of Geophysical Research*, *106*(A7), 13,191–13,201. https://doi.org/10.1029/2000JA000275

Santolík, O., Macúšová, E., Kolmašová, I., Cornilleau-Wehrlin, N., & Conchy, Y. (2014). Propagation of lower-band whistler-mode waves in the outer Van Allen belt: Systematic analysis of 11 years of multi-component data from the Cluster spacecraft. *Geophysical Research Letters*, *41*, 2729–2737. https://doi.org/10.1002/2014GL059815

Santolík, O., Němec, F., Gereová, K., Macúšová, E., De Conchy, Y., & Cornilleau-Wehrlin, N. (2004). Systematic analysis of equatorial noise below the lower hybrid frequency. *Annales Geophysicae*, *22*, 2587–2595. https://doi.org/10.5194/angeo-22-2587-2004

Santolík, O., Němec, F., Parrot, M., Lagoutte, D., Madrias, L., & Berthelier, J. (2006). Analysis methods for multi-component wave measurements on board the DEMETER spacecraft. *Planetary and Space Science*, *54*(5), 512–527. https://doi.org/10.1016/j.pss.2005.10.020

Santolík, O., & Parrot, M. (1996). The wave distribution function in a hot magnetospheric plasma: The direct problem. *Journal of Geophysical Research*, *101*(A5), 10,639–10,651. https://doi.org/10.1029/95JA03510

Santolík, O., & Parrot, M. (1998). Propagation analysis of electromagnetic waves between the helium and proton gyrofrequencies in the low-altitude auroral zone. *Journal of Geophysical Research*, *103*(A9), 20,469–20,480. https://doi.org/10.1029/98JA01386

Santolík, O., & Parrot, M. (1999). Case studies on the wave propagation and polarization of ELF emissions observed by Freja around the local proton gyrofrequency. *Journal of Geophysical Research*, *104*(A2), 2459–2475. https://doi.org/10.1029/1998JA900045

Santolík, O., & Parrot, M. (2000). Application of wave distribution function methods to an ELF hiss event at high latitudes. *Journal of Geophysical Research*, *105*(A8), 18–885. https://doi.org/10.1029/2000JA900029

Santolík, O., Parrot, M., Inan, U., Burešová, D., Gurnett, D., & Chum, J. (2009). Propagation of unducted whistlers from their source lightning: A case study. *Journal of Geophysical Research*, *114*, A03212. https://doi.org/10.1029/2008JA013776

Santolík, O., Parrot, M., & Lefeuvre, F. (2003). Singular value decomposition methods for wave propagation analysis. *Radio Science*, *38*(1), 1010. https://doi.org/10.1029/2000RS002523

Santolík, O., Parrot, M., & Němec, F. (2016). Propagation of equatorial noise to low altitudes: Decoupling from the magnetosonic mode. *Geophysical Research Letters*, *43*, 6694–6704. https://doi.org/10.1002/2016GL069582

Sazhin, S., & Hayakawa, M. (1992). Magnetospheric chorus emissions: A review. *Planetary and space science*, *40*(5), 681–697. https://doi.org/10.1016/0032-0633(92)90009-D

Singh, A. K., Singh, S., Singh, R., Gokani, S. A., Singh, A. K., Siingh, D., & Lichtenberger, J. (2014). Whistlers detected and analyzed by Automatic Whistler Detector (AWD) at low latitude Indian stations. *Journal of Atmospheric and Solar-Terrestrial Physics*, *121*, 221–228. https://doi.org/10.1016/j.jastp.2014.03.001

Smith, R., & Angerami, J. (1968). Magnetospheric properties deduced from OGO 1 observations of ducted and nonducted whistlers. *Journal of Geophysical Research*, *73*(1), 1–20. https://doi.org/10.1029/JA073i001p00001

Starks, M., Quinn, R., Ginet, G., Albert, J., Sales, G., Reinisch, B., & Song, P. (2008). Illumination of the plasmasphere by terrestrial very low frequency transmitters: Model validation. *Journal of Geophysical Research*, *113*, A09320. https://doi.org/10.1029/2008JA013112

Storey, L. (1953). An investigation of whistling atmospherics. *Philosophical Transactions of the Royal Society of London A: Mathematical, Physical and Engineering Sciences*, *246*(908), 113–141. https://doi.org/10.1098/rsta.1953.0011

Tao, X., Bortnik, J., & Friedrich, M. (2010). Variance of transionospheric VLF wave power absorption. *Journal of Geophysical Research*, *115*, A07303. https://doi.org/10.1029/2009JA015115

Thorne, R., Horne, R., & Meredith, N. (2006). Comment on "On the origin of whistler mode radiation in the plasmasphere" by Green others. *Journal of Geophysical Research*, *111*, A09210. https://doi.org/10.1029/2005JA011477

Voss, H., Walt, M., Imhof, W., Mobilia, J., & Inan, U. (1998). Satellite observations of lightning-induced electron precipitation. *Journal of Geophysical Research*, *103*(A6), 11,725–11,744. https://doi.org/10.1029/97JA02878

Walker, A. (1976). The theory of whistler propagation. *Reviews of Geophysics*, *14*(4), 629–638.